ELSEVIER

Neural specificity of acupuncture stimulation from support vector machine classification analysis

Ting Xue[a], Lijun Bai[b], Shangjie Chen[c], Chongguang Zhong[b], Yuanyuan Feng[b], Hu Wang[b], Zhenyu Liu[b], Youbo You[b], Fangyuan Cui[d], Yanshuang Ren[e], Jie Tian[a,b,*], Yijun Liu[f]

[a]Life Sciences Research Center, School of Life Sciences and Technology, Xidian University, Xi'an 710071, China
[b]Medical Image Processing Group, Institute of Automation, Chinese Academy of Sciences, Beijing 100190, China
[c]Baoan Hospital, Southern Medical University, Shenzhen 518101, China
[d]Department of neurology, Dongzhimen Hospital Affiliated to Beijing University of Chinese Medicine, Beijing 100700, China
[e]Department of Radiology, Guanganmen Hospital, Chinese Academy of Traditional, Medicine, Beijing 100053, China
[f]McKnight Brain Institute, Departments of Psychiatry and Neuroscience, University of Florida, FL, USA

Abstract

Acupoint specificity, as a crucial issue in acupuncture neuroimaging studies, is still a controversial topic. Previous studies have generally adopted a block-based general linear model (GLM) approach, which predicts the temporal changes in the blood oxygenation level-dependent signal conforming to the "on–off" specifications. However, this method might become impractical since the precise timing and duration of acupuncture actions cannot be specified a priori. In the current study, we applied a data-driven multivariate classification approach, namely, support vector machine (SVM), to explore the neural specificity of acupuncture at gall bladder 40 (GB40) using kidney 3 (KI3) as a control condition (belonging to different meridians but the same nerve segment). In addition, to verify whether the typical GLM approach is sensitive enough in exploring the neural response patterns evoked by acupuncture, we also employed the GLM method to the same data sets. The SVM analysis detected distinct neural response patterns between GB40 and KI3 — positive predominantly for the GB40, while negative following the KI3. By contrast, group analysis from the GLM showed that acupuncture at these different acupoints can both evoke similar widespread signal decreases in multiple brain regions, and most of these regions were spatially overlapped, mainly distributing in the limbic and subcortical structures. Our findings may provide additional evidence to support the specificity of acupuncture, relevant to its clinical efficacy. Moreover, we also proved that GLM analysis is prone to be susceptible to errors and is not appropriate for detecting neural response patterns evoked by acupuncture stimulation.
Crown Copyright © 2011 Published by Elsevier Inc. All rights reserved.

Keywords: Acupuncture specificity; Functional magnetic resonance imaging (fMRI); Support vector machine analysis (SVM)

1. Introduction

As one of the best known complementary and alternative therapies, acupuncture has gained great popularity not only in China but also in the United States as well as other parts of the Western world. In clinical practice, acupuncture has been proven to be efficacious for some diseases, such as pain, nausea and vomiting [1]. Nevertheless, the scientific explanation regarding the physiological mechanisms of acupuncture stimulation has not been found.

Acupoint specificity, lying at the core of the Traditional Chinese Medicine, still faces many controversies, and scientific evidence regarding the specificity of acupuncture modulatory effects splits in both the positive and negative sides. A group of studies has reported that acupuncture stimulation at several traditional "vision-related" acupoints can selectively evoke neural responses in the occipital (visual) cortex, while such neural activities do not emerge after stimulation at a nearby nonacupoint [2,3]. However, this conclusion can hardly be supported by other researches. One recent investigation has indicated that acupuncture stimulation at vision-related acupoints and nonacupoint can

* Corresponding author. Institute of Automation, Chinese Academy of Sciences, Zhong Guancun, Beijing 100190, China. Tel.: +86 010 82618465; fax: +86 010 62527995.
 E-mail addresses: tian@ieee.org, tian@fingerpass.net.cn (J. Tian).

both produce similar widespread functional magnetic resonance imaging (fMRI) signal deactivations in the occipital cortex [4]. This result does not support the specificity of vision-related acupoints. In addition, some researchers also reported that stimulation at nonacupoints or treatment-irrelevant acupoints shared the deactivated regions of the limbic system and subcortical structures, such as the hippocampus, parahippocampus, anterior cingulate cortex, precuneus, medial prefrontal cortex, amygdala and temporal pole [5–7]. They further inferred that such decreased neural activities in the limbic system and subcortical structures may underlie the central nervous system effects of acupuncture. As aforementioned above, these conflicting results indicate that acupoint specificity is still a controversial issue; further work is needed to clarify whether neural responses are as specific as the purported indication of different acupoints.

The extant studies on neural responses evoked by acupuncture have generally adopted a multiblock experimental paradigm and general linear model (GLM) approach [4–7]. With this approach, a specific stimulus sequence (i.e., design matrix) is used to define a ideal hemodynamic response function (HRF), which is convolved with the experimental paradigm and produces predictors of the blood oxygenation level-dependent (BOLD) response [8]. The inferences derived from GLM estimates are limited by the design of the experimental paradigm and whether the stimuli are under relatively precise experimental control (i.e., they can be turned on and off repeatedly) [9]. For a block-designed fMRI paradigm, the temporal changes in the BOLD signal as predicted by the GLM conform to the "on–off" specifications set by the experimenter. However, abundant clinical reports have demonstrated that acupuncture effects can sustain beyond acupuncture needling being terminated [10]. Since acupuncture effects may be of relatively long duration [11,12], the temporal profile of BOLD response to acupuncture may violate the "on–off" assumptions of block-designed GLM estimates. Further group analysis may be susceptible to errors of statistical significance. In addition, for all the participants, the time series in each voxel is fit to one single model which contains the regressors related to the expected BOLD signal changes [8,13]. It is obvious that GLM is a univariate approach which seems to be not taking advantage of the spatially distributed information contained in fMRI data to give a better understanding of neural activities. Moreover, GLM does not take into account individual differences, while such differences might be significant for participants recruited in acupuncture studies and may ultimately produce a negative impact on neuroimaging results [14,15]. Therefore, we proposed that model-based GLM approach may not be sensitive enough to detect the neural activities in response to acupuncture stimuli, and it is not appropriate for exploring neural mechanisms underlying the theoretical basis of acupuncture application.

In the current study, we took a data-driven support vector machine (SVM) [16] multivariate classification approach to probe neural responses evoked by acupuncture stimuli. In contrast to other classification approaches, SVM has already shown to provide better generalization performance [17]. More importantly, as one of the data-driven approaches, SVM did not specify any constraints on the shape of BOLD signal changes due to stimulation. By performing multivariate classification of the neuroimaging volumes belonging to two classes (acupuncture stimulation vs. no acupuncture stimulation), SVM could assess each individual's BOLD signal temporal fluctuations associated with acupuncture stimuli [18,19], namely, temporal fluctuations of spatial discriminance patterns [spatial discriminance pattern temporal profile (SDPtp)], characterizing the temporal dynamics of active brain areas. It has been demonstrated that SDPtp could reflect the task-induced temporal fluctuations of BOLD signal changes [18]; then it is sensible to apply SDPtp for modeling HRF changes elicited by acupoint stimulation. Since SDPtp was extracted based on each individual, it might provide a solution for individual differences. In addition, considering the SVM classification is based on the whole image volume, this approach is inherently multivariate and may make use of the spatially distributed information contained in fMRI data as much as possible. As discussed above, we speculated that data-driven SVM multivariate classification approach may be more appropriate for acupuncture studies, and it can be used as an alternative method for probing neural mechanisms of acupuncture stimulation.

We applied the SVM classification approach to elucidate the neurophysiologic correlates of acupuncture stimulation at gall bladder 40 (GB40) (Qiuxu, an important acupoint for pain relief in clinical settings), using kidney 3 (KI3) (Taixi, an acupoint for treatment of cognitive impairments) as a control condition. Both GB40 and KI3 are innervated by the same spinal nerve, while belonging to different meridians. We tested whether there were neural differences between GB40 and KI3. To verify whether typical GLM analysis is sensitive enough for detecting neural activities evoked by acupuncture stimulation, we also applied GLM method to the same data sets.

2. Methods and materials

2.1. Subjects

Twelve Chinese healthy volunteers (9 male, ages of 21–26 years) were recruited to this study. According to the Edinburgh Handedness Inventory [20], the subjects were all right-handed. All the participants were acupuncture naive and did not have a history of major medical illnesses, head trauma and neuropsychiatric diseases. The subjects had not used any prescription medications within the last month. After a brief description of the study was given to all subjects, written informed consent was obtained. The experiments were conducted in accordance with the Declaration of Helsinki.

2.2. Experimental paradigm

Each subject participated in two fMRI scanning runs for acupuncture at GB 40 and KI 3 separately. To eliminate the sustained effects of acupuncture, a 1-week interval was interposed between these two consecutive scans [10]. The experimental paradigm was an on-off block design (shown in Fig. 1B) that included 1 min of rest scanning at the beginning; the three stimulations' epoch was then separated by two intervals of 1-min "rest" period. The total scanning time was 6 min per run.

Before scanning, all subjects were briefly informed of acupuncture and fMRI to reduce anxiety about the experiments. Acupuncture was performed at acupoints GB40 (Qiuxu, located in a depression at the anteroinferior side of lateral malleolus and lateral to long extensor muscle of toes) and KI3 (Taixi, located in a depression between medial malleolus and heel tendon) (shown in Fig. 1A). Subjects were not informed of the order in which these two acupuncture manipulations would be performed and were asked to keep their eyes closed to prevent them from actually observing the procedures. The presentation sequence of these two protocols was randomized across the fMRI runs, and the order of presentation was counterbalanced across subjects. Acupuncture stimulation was delivered using a sterile disposable stainless steel needle. Considering the anatomical differences, the needling depth ranged from 2.5 to 3.0 cm for KI3 and 2.0 to 2.5 cm for GB40. Stimulation was then delivered by a balanced "tonifying and reducing" technique and rotated manually clockwise and counterclockwise for 1 min at a rate of 60 times per min. The procedure was performed by a single experienced acupuncturist using
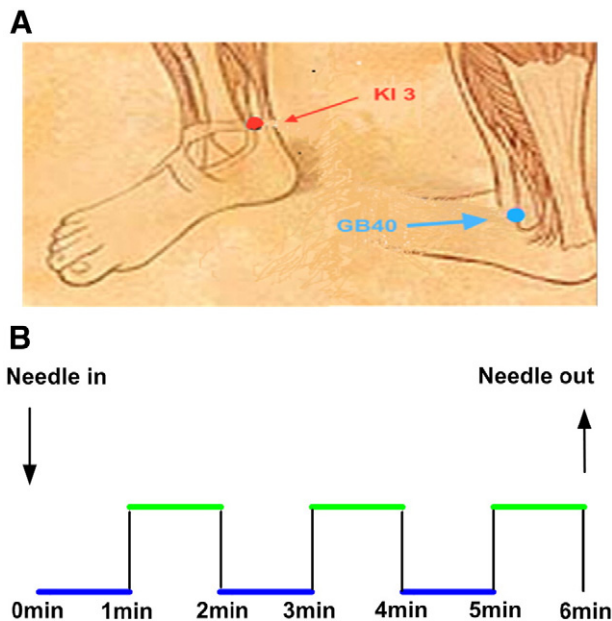

Fig. 1. Experimental design: (A) illustration of anatomical locations of two acupoints: GB40 (Qiuxu)and KI3 (Taixi); (B) functional run incorporated the block design paradigm with three cycles.

the same method of acupuncture administration in the two scanning runs. During the experiment, the subjects were told to remain relaxed without engaging in any mental tasks.

At the end of each scanning, the subjects were asked to quantify their experience (or "deqi") of the aching, throbbing, soreness, heaviness, fullness, warmth, numbness, tingling, dull or sharp pain and any other sensations they felt during the scan [4,6]. The sensation rates from 0 to 10 (0=*no sensation*, 1–3=*mild*, 4–6=*moderate*, 7–8=*strong*, 9=*severe* and 10=*unbearable sensation*).

2.3. Data acquisition and preprocessing

All experiments were performed at a 3-T MRI system (ACS-NT15, Gyroscan, Philips Medical Systems) equipped with a standard whole head coil. A custom-built head holder was used to prevent head movements. Functional MR images were obtained using a gradient echo T2*-weighted pulse sequence with repetition time (TR)=4000 ms, echo time (TE)=50 ms, matrix=64×64, field of view (FOV)=230 mm×230 mm and flip angle (FA)=90°. Then 30 slices (5-mm thickness, 0-mm gap) oriented parallel to the AC-PC line were collected to cover the whole brain. After the functional run, high-resolution structural information on each subject was acquired using three-dimensional MRI sequences with a voxel size of 1 mm^3 for anatomical localization (TR=2510 ms, TE=15 ms, matrix=384×512, FOV=230 mm×230 mm, FA=30°, thickness=5 mm).

All preprocessing steps were carried out using Matlab 7.6.0 (2008a) (Math works Inc., Natick, MA, USA) and in batch mode with Statistical Parametric Mapping software (SPM5, http://www.fil.ion.ac.uk). The first five volumes of each session were discarded to allow for T1 equilibration effects [21]. All the remaining volumes were slice-timed and then realigned to correct for head motions using the least squares minimization. None of the subjects had head movements exceeding 1 mm on any axis and head rotation greater than 1°. The image data were further processed with spatial normalization based on the Montreal Neurological Institute space and resampled at 4 mm×4 mm×4 mm. A mean image created from the realigned volumes was co-registered with the subject's individual structural T1-weighted volume image. Finally, the images were smoothed with a 6-mm full-width at half-maximum Gaussian kernel.

2.4. Dimensionality reduction

To reduce computational burden, a mask generated from the raw echo-planar imaging (EPI) images was first used to remove voxels out of gray matter. Then standard singular vector decomposition method was applied to represent the data in a space of smaller dimensionality without loss of information. For each run, an original image volume $s_i=(s_{1i}, s_{2,i},..., s_{N,i})$, $i=1, 2,..., L$ can be represented as a coefficient vector $x_i=(x_{1,i}, x_{2,i},..., x_{L,i})$, $i=1, 2,..., L$ [22]. Here, N and L are the number of voxels in gray matter and the number of scans during one session. Then the following SVM

multivariate classification approach will be carried out with the representation coefficient vector series $X=(x_1, x_2,..., x_{Li})$.

2.5. Linear SVM classification and SDP extraction

Since fMRI data are linearly separable (in high dimension with few data points), the SVM based on linear kernel is sufficient to extract an optimal hyperplane separating the image volumes of two contrasting conditions (the situation here, −1 indicates no acupuncture stimulation, while +1 indicates acupuncture stimulation). With the training samples $\{x_i, y_j\}$, $i=1, 2,..., L$, $y_j \in \{-1,+1\}$, a linear SVM was performed using SVMTRAIN function from the MATLAB 7.6 bioinformatics toolbox. Support vector machine could directly extract a hyperplane $w·x+b=0$ in the feature space R^L with the largest margin. Then a spatial discriminance map (SDM) could be obtained by projecting the weight vector w back to the original image space. The SDM represents an image volume with the most discriminating regions; and spatial brain discriminance patterns (SDPs) represent the patterns carried in SDM. For a detailed description of the SVM, see Ref. [23].

2.6. SDPtp extraction

It has been proved that the SDPtp could reflect task-induced temporal fluctuations of BOLD signal changes [18]; therefore, it is sensible to apply SDPtp for modeling HRF changes evoked by acupuncture stimuli. A natural measure for SDPtp is the distance of each representing coefficient vector x_i to the separating hyperplane [18]. In this study, we used the signed distance $D_i = \frac{w·x_i + b}{\|w\|}$ as a measure of SDPtp. Here, w is the weight vector normal to the hyperplane, $\|w\|$ is the Euclidean norm of w and b is the offset. A sequence of signed distances $\{D_i, i=1,..., L\}$ would be arranged according to the acquisition time of the corresponding image volumes in a session. Then the final SDPtp $D=(D_1, D_2,..., D_L)$ was obtained to model HRF changes evoked by acupuncture stimuli.

2.7. Activity detection and random effects analysis

For each participant, the voxels activated by acupuncture stimuli could be identified using the same method as that used in GLM approach, just replacing HRF with SDPtp. So far, we have considered only single neural activity detection (level one); to provide a population inference, random effects (RFX) analysis was carried out to assess the between-subject variability of the brain activation [24]. The RFX of the individual-level neural activity could be performed using a one-sample t test (under the null hypothesis that there is no activation). Statistical significance was thresholded at $P<.005$ (uncorrected) and a minimum cluster size of five voxels.

2.8. Conventional GLM analysis

To verify whether model-based GLM is sensitive enough for exploring neural activities elicited by acupuncture stimuli, we also performed GLM analysis to the same data sets. The signal intensities with the needle at rest before, between and after the needle manipulation periods served as the baseline for the assessment of changes in signal intensity induced by needle stimulation. The statistical analyses were performed subsequently at both the individual level and group level (one-sample t test). To be the same with SVM analysis, statistical significance was also thresholded at $P<.005$ (uncorrected) and a minimum cluster size of five voxels.

3. Results

3.1. Psychophysical responses

The prevalence of these sensations was expressed as the percentage of the individuals in the group that reported the sensation (shown in Fig. 2A). A statistical analysis found no significant difference between the GB40 group and KI3 group in regard to the prevalence of these sensations (paired t test, $P>.05$).The stimulus intensity was expressed as the average score±S.E. (shown in Fig. 2B). The average stimulus intensities
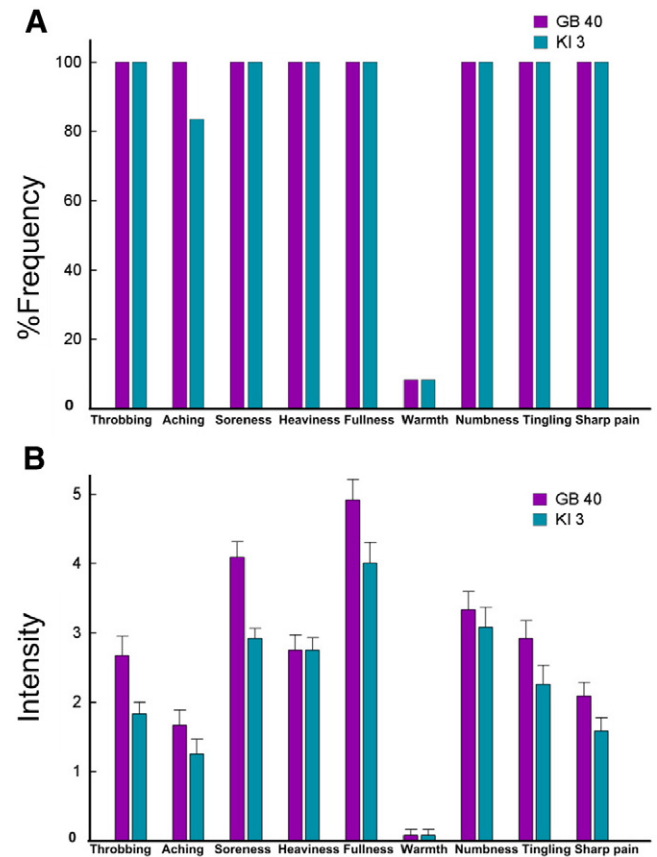

Fig. 2. Results of psychophysical analysis: (A) percentage of subjects who reported having experienced the given sensations; (B) the intensity of the reported sensations measured by an averaged score (with standard error bars) on a scale from 0 (denoting no sensations) to 10 (denoting an unbearable sensation).

Table 1
Group results of GB40 and KI3 obtained by SVM (*P*<.005, uncorrected with a minimum cluster size of five contiguous voxels)

Regions	GB40						KI3					
	Hem	Talairach			*t*	*V*	Hem	Talairach			*t*	*V*
		x	*y*	*z*	value	voxels		*x*	*y*	*z*	value	voxels
Insula	R	42	−20	0	4.72	90	R	42	−23	−2	−4.92	56
	L						L	−34	−16	21	−4.48	21
Red nucleus	R	6	−16	−8	4.31	15	R					
	L	−4	−18	−10	6.56	91	L					
Thalamus	R	14	−8	6	5.27	21	R	22	−33	5	−6.69	41
	L	−16	−12	6	4.38	17	L					
Amygdala	R	28	−4	−12	4.61	23	R					
	L						L	−28	−5	−15	−4.23	34
Uvula	R						R	4	−71	−28	−3.76	12
	L	−8	−73	−32	−3.37	17	L					
Medial frontal	R						R	12	11	−17	−4.68	65
	L						L	−4	49	16	−4.93	75
Posterior cingulate cortex	R						R	4	−59	25	−5.79	76
	L						L	−4	−65	16	−5.22	66
Anterior cingulate cortex	R						R	2	31	0	−3.53	19
	L						L	−2	33	0	−4.55	47

(mean±S.E.) were 2.72±0.65 at GB40 and 2.19±0.57 at KI3. Significant differences could be found in soreness, fullness, throbbing, tingling and sharp pain (paired *t* test, *P*<.05).

3.2. SVM results

Group results obtained from SVM analysis displayed distinct neural response patterns between acupuncture stimulation at GB40 and KI3. Acupuncture stimulation at GB40 produced predominantly signal increases in the insula, red nucleus, thalamus and amygdala (*P*<.005, uncorrected), with limited extent of signal decreases only located in the uvula (Table 1). By contrast, acupuncture at KI3 elicited more extensive decreased neural responses in the medial frontal gyrus, posterior cingulate cortex, thalamus and anterior cingulate cortex (shown in Fig. 3A).

We also performed a paired *t* test (KI3 vs. GB40) to further verify statistically significant differences between stimulation at GB40 and KI3. Significant differences could be found in the left insula (BA13), inferior temporal gyrus (BA20), superior frontal gyrus (BA9) and cingulate gyrus (BA31) (*P*<.005, uncorrected and a minimum cluster size of five voxels) (shown in Fig. 4).

3.3. GLM results

Group results derived from the conventional GLM analysis (*P*<.005, uncorrected) showed that acupuncture stimulation at GB40 and KI3 can both evoke similar widespread signal decreases in multiple brain regions (shown in Fig. 3B). Most of these regions were spatially overlapped and mainly distributed in the limbic and subcortical structures, such as the hippocampus, parahippocampus, anterior cingulate cortex, precuneus, medial prefrontal cortex, amygdala and temporal pole.

4. Discussion

In this paper, we applied an SVM multivariate classification approach to explore the neural specificity of acupuncture at GB40 using KI3 as a control condition. Group results from SVM analysis presented that acupuncture stimulation at GB40 can evoke prominently increased neural responses in the insula, thalamus and red nucleus, while there were more decreased activations in the medial frontal gyrus and subcortical structures following acupuncture at KI3. These results may suggest potentially selective efficacy-related neural actions in response to acupuncture at different acupoints. More importantly, our findings may provide additional evidence to support the specificity of acupuncture modulation effects underlying the theoretical basis of acupuncture application.

Group results obtained from SVM analysis displayed prominently opposite neural response patterns between acupuncture stimulation at GB40 and KI3. Following acupuncture at GB40, results from SVM analysis presented saliently positive signal changes in the insula, thalamus and red nucleus. Anatomical studies have revealed that the insula cortex has wide connections with the somatosensory areas, anterior cingulated cortex, amygdaloid body, prefrontal cortex, hypothalamus and other brain structures [25]. Its abundant connections and functional interface between the limbic system and the neocortex place it in a unique position to assign significance to the sensory information it receives and to possibly effect decisions and subsequent behavior [26]. It could be speculated that the insula may play a key role in mediating the influence of human expectation on the perception of pain. The thalamus and red nucleus, as parts of subcortical nuclei, have also been proven to be generally involved in regulation of pain transmission [27]. Since the regions activated by GB40 were partially overlapped with
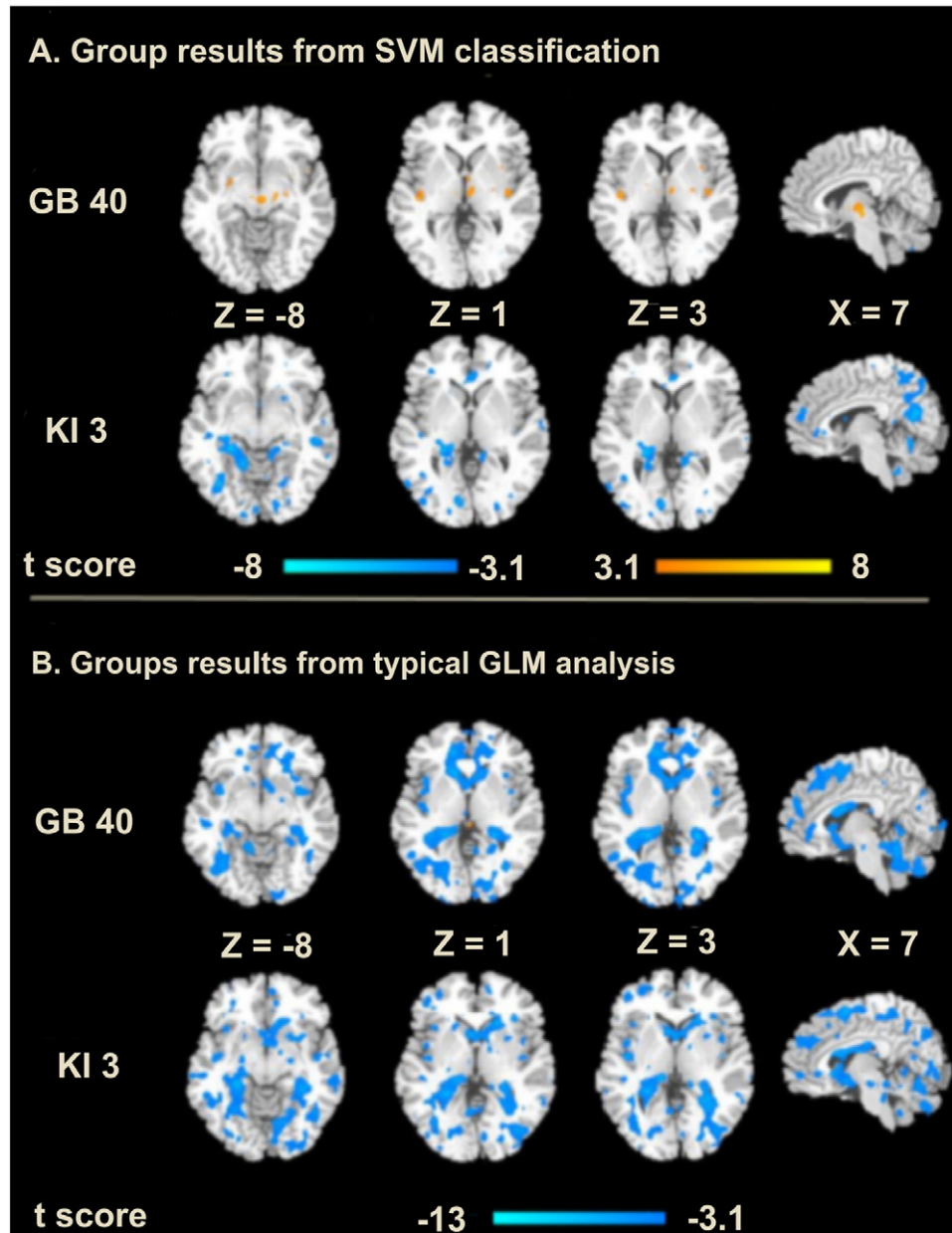
Fig. 3. Neural response patterns for acupuncture at GB40 and KI3. (A) Results from SVM analysis showed that acupuncture at GB40 produced predominantly signal increases. By contrast, acupuncture at KI3 elicited more extensive decreased neural responses. (B) Group analysis of typical GLM approach. Statistical significance was thresholded at $P<.005$ (uncorrected) and a minimum cluster size of five voxels.

the neural pathways for pain, and GB40 has been used clinically to treat pain-related diseases, such as low back pain [28], it can be speculated that GB40 may have certain effects in relation to analgesic activity. By contrast, acupuncture at KI3 produced extensive signal decreases in the thalamus, medial frontal gyrus, posterior cingulate cortex and anterior cingulate cortex. It has been demonstrated that these regions are more engaged in cognitive-related neural activity [29]. In clinical practice, KI3 has also been proven to have modulatory effects on cognitive-related diseases [30], such as Alzheimer's disease. These results suggested that KI3 may play a role, at least to some extent, in regulating

cognitive functions. From these observations, we drew a conclusion that acupuncture at these two different acupoints could elicit distinct neural response patterns. We further proposed that specific neural substrates might underlie the differential acupuncture actions.

To verify whether model-based GLM approach is sensitive enough to detect neural activities elicited by acupuncture stimuli, we also applied the GLM method to the same data sets. Intriguingly, group results showed that acupuncture at these two points can both evoke similar widespread signal decreases in multiple brain regions. Most of these regions were spatially overlapped and mainly
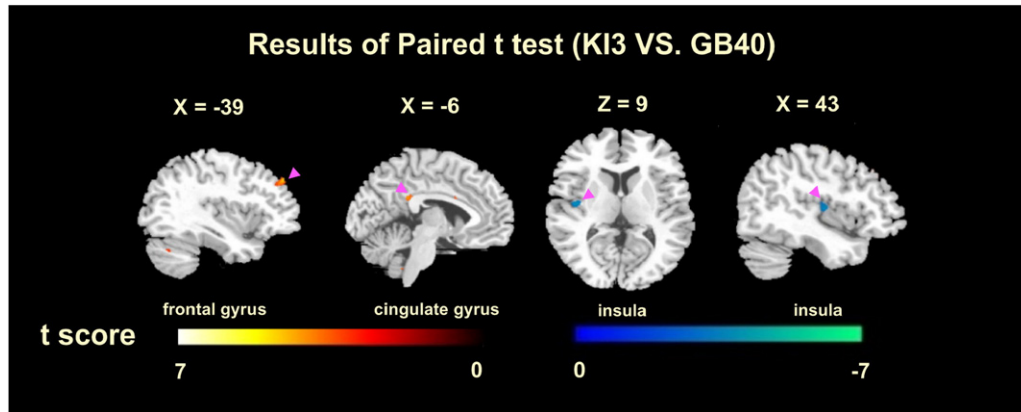
Fig. 4. Results of paired *t* test of KI3 vs. GB40 with *P*<.005 (uncorrected) and a minimum cluster size of five voxels.

distributed in the limbic and subcortical structures. We speculated that the findings of large overlapping deactivated brain areas might be attributed to the inappropriate application of model-based GLM analysis. For a block-designed paradigm, the temporal changes in the BOLD signal as predicted by the GLM conform to the "on–off" specifications. However, abundant clinical reports as well as literatures have demonstrated that acupuncture effects can sustain beyond acupuncture needling being terminated [9,10]. That is to say, there might still be acupuncture effects during the "off" periods. Considering that GLM analysis is based on the subtraction principle, the subtraction of the average BOLD signal in the "off" periods from that in the acupuncture-stimulus epoch ("on" periods) might ultimately lead to such decreased signal findings. Therefore, we proposed that model-based GLM approach might be susceptible to error results and is not appropriate for acupuncture studies.

5. Conclusion

In the current study, we applied an SVM classification approach to elucidate the neural response patterns evoked by acupuncture stimulation at GB40 using KI3 as a control point. Group results showed distinct patterns of neural response: predominantly positive for GB40, while negative for KI3. Our findings may provide additional evidence to support the specificity of acupuncture modulation effects underlying the theoretical basis of acupuncture application. Moreover, we also show that conventional GLM analysis is insensitive to detect neural activities evoked by acupuncture stimuli, and we further propose that GLM is not appropriate for probing the neural mechanisms underlying acupuncture efficacies.

References

[1] Al-Sadi M, Newman B, Julious S. Acupuncture in the prevention of postoperative nausea and vomiting. Anaesthesia 1997;52:658–61.

[2] Lee H, Park HJ, Kim SA, Lee HJ, Kim MJ, Kim CJ, et al. Acupuncture stimulation of the vision-related acupoint (bl-67) increases c-fos expression in the visual cortex of binocularly deprived rat pups. Am J Chin Med 2002;30:379–85.

[3] Li G, Cheung R, Ma Q, Yang E. Visual cortical activations on fMRI upon stimulation of the vision-implicated acupoints. Neuroreport 2003;14:669.

[4] Kong J, Kaptchuk TJ, Webb JM, Kong JT, Sasaki Y, Polich GR, et al. Functional neuroanatomical investigation of vision-related acupuncture point specificity — a multisession fMRI study. Hum Brain Mapp 2009;30:38–46.

[5] Hui KK, Liu J, Makris N, Gollub RL, Chen AJ, Moore CI, et al. Acupuncture modulates the limbic system and subcortical gray structures of the human brain: evidence from fMRI studies in normal subjects. Hum Brain Mapp 2000;9:13–25.

[6] Hui K, Liu J, Marina O, Napadow V, Haselgrove C, Kwong K, et al. The integrated response of the human cerebro-cerebellar and limbic systems to acupuncture stimulation at st 36 as evidenced by fMRI. Neuroimage 2005;27:479.

[7] Fang J, Jin Z, Wang Y, Li K, Kong J, Nixon EE, et al. The salient characteristics of the central effects of acupuncture needling: limbic–paralimbic–neocortical network modulation. Hum Brain Mapp 2009;30:1196–206.

[8] Friston KJ, Holmes AP, Poline JB, Grasby PJ, Williams SC, Frackowiak RS, et al. Analysis of fMRI time-series revisited. Neuroimage 1995;2:45–53.

[9] Bai L, Qin W, Tian J, Liu P, Li L, Chen P, et al. Time-varied characteristics of acupuncture effects in fMRI studies. Hum Brain Mapp 2009;30:3445–60.

[10] Beijing College of Traditional Chinese Medicine, Shanghai College of Traditional Chinese Medicine, Nanjing College of Traditional Chinese Medicine, The Acupunture Institute of the Academy of Traditional

Chinese Medicine. Essentials of Chinese acupuncture. Beijing: Foreign Language Press; 1980.

[11] Bai L, Qin W, Liang J, Tian J, Liu Y. Spatiotemporal modulation of central neural pathway underlying acupuncture action: a systematic review. Curr Med Imaging Rev 2009;5:167–73.

[12] Bai L, Yan H, Li L, Qin W, Chen P, Liu P, et al. Neural specificity of acupuncture stimulation at pericardium 6: evidence from an fMRI study. J Magn Reson Imaging 2010;31:71.

[13] Josephs O, Turner R, Friston K. Event-related fMRI. Hum Brain Mapp 1997;5:243.

[14] Bennett C, Miller M. How reliable are the results from functional magnetic resonance imaging? Ann N Y Acad Sci 2010;1191:133.

[15] Kong J, Gollub RL, Webb JM, Kong JT, Vangel MG, Kwong K. Test–retest study of fMRI signal change evoked by electroacupuncture stimulation. Neuroimage 2007;34:1171–81.

[16] Vapnik V. The nature of statistical learning theory. New York: Springer Verlag; 2000.

[17] Kim K, Jung K, Park S, Kim H. Support vector machines for texture classification. IEEE Trans Pattern Anal Mach Intell 2002;24:1542–50.

[18] Wang Z. A hybrid SVM–GLM approach for fMRI data analysis. Neuroimage 2009;46:608–15.

[19] Mourao-Miranda J, Friston KJ, Brammer M. Dynamic discrimination analysis: a spatial–temporal SVM. Neuroimage 2007;36:88–99.

[20] Oldfield R. The assessment and analysis of handedness: the Edinburgh inventory. Neuropsychologia 1971;9:97.

[21] Castelli F, Glaser D, Butterworth B. Discrete and analogue quantity processing in the parietal lobe: a functional MRI study. Proc Natl Acad Sci U S A 2006;103:4693.

[22] Vetterling W, Teukolsky S, Press W, Flannery B. Numerical recipes example book (c++). Cambridge: Univ. Press; 2002.

[23] Scholkopf B, Smola A. Learning with kernels. Cambridge: MIT Press; 2002.

[24] Holmes A, Friston K. Generalisability, random effecrts and population inference. Neuroimage. Abstracts of the Fourth International Conference on Functional Mapping of the Human Brain; 1998. p. 7.

[25] Chikama M, McFarland N, Amaral D, Haber S. Insular cortical projections to functional regions of the striatum correlate with cortical cytoarchitectonic organization in the primate. J Neurosci 1997;17:9686.

[26] Casey K. Forebrain mechanisms of nociception and pain: analysis through imaging. Proc Natl Acad Sci U S A 1999;96:7668.

[27] Dunckley P, Wise R, Fairhurst M, Hobden P, Aziz Q, Chang L, et al. A comparison of visceral and somatic pain processing in the human brainstem using functional magnetic resonance imaging. J Neurosci 2005;25:7333.

[28] MacPherson H, Thorpe L, Thomas K, Campbell M. Acupuncture for low back pain: traditional diagnosis and treatment of 148 patients in a clinical trial. Complement Ther Med 2004;12:38–44.

[29] Duffy JD, Campbell III JJ. The regional prefrontal syndromes: a theoretical and clinical overview. J Neuropsychiatry Clin Neurosci 1994;6:379–87.

[30] Lee MS, Shin BC, Ernst E. Acupuncture for alzheimer's disease: a systematic review. Int J Clin Pract 2009;63:874–9.